Supplemental Material: Nonlinear polariton fluids in a flat band reveal discrete gap solitons

V. Goblot,[1,*] B. Rauer,[1,2] F. Vicentini,[3] A. Le Boité,[3] E. Galopin,[1] A. Lemaître,[1] L. Le Gratiet,[1] A. Harouri,[1] I. Sagnes,[1] S. Ravets,[1] C. Ciuti,[3] A. Amo,[4] and J. Bloch[1]

[1] *Centre de Nanosciences et de Nanotechnologies (C2N), CNRS, Université Paris-Sud, Université Paris-Saclay, 91120 Palaiseau, France*
[2] *Vienna Center for Quantum Science and Technology, Atominstitut, TU Wien, Stadionallee 2, 1020 Vienna, Austria*
[3] *Laboratoire Matériaux et Phénomènes Quantiques, Université de Paris, CNRS, 75013 Paris, France*
[4] *Laboratoire de Physique des Lasers Atomes et Molécules (PhLAM), 59000 Lille, France*

I. RESONANT EXCITATION OF THE FLAT BAND MODES

To determine the optimal excitation scheme for the resonant drive of the flat band, we study the momentum-space resolved photoluminescence (PL) of the flat band modes. This pattern can be obtained by spectrally filtering the emission, measured under weak non-resonant pumping, at the flat band energy. The (k_x, k_y) map of the emission is then reconstructed from spectra measured at different values of k_y, such as the one shown in Fig. 1(c) of the main text. The result is presented in Fig. S1(b): the intensity is zero at the center of the Brillouin zone (BZ) ($(k_x, k_y) = 0$), and is maximal at the BZ edges ($k_x = \pi/a$). This reflects the antisymmetric nature of the flat band eigenmodes (opposite phase on A, C pillars). Thus, to ensure efficient coupling to the polariton states in the flat band, the pumping beam is tilted from normal incidence by 5.0° along the x direction, corresponding to the edge of the first BZ.

The real-space PL at the energy of the flat band can also be obtained with a similar method (spectral filtering of the real-space PL) and is shown at the top of Fig. S1(b). As expected due to geometric frustration, we measure vanishing intensity on B sites.

Let us comment briefly on the consequence of exciting the flat band at the BZ edge. When the wave-vector of the driving field is equal to $k = \pi/a$, it imposes a phase difference of exactly π between neighboring unit cells. The opposite sign on C sites in neighboring unit cells leads to a destructive interference on A sites. As an illustration, Fig. S1(c,d) shows calculated real- and momentum-space emission pattern of two different localized eigenstates: a single plaquette $|f_n\rangle$, and a linear superposition of four plaquettes, of same magnitude but alternating sign on neighboring unit cells, which can be written $\sum_{j=0}^{3}(-1)^j|f_{n+j}\rangle$. To compute these radiation patterns, we use a simplistic description of the eigenfunctions of the chain of pillars: we consider a Gaussian-shaped orbital per pillar (corresponding to the s mode). To construct a given wave function, we assign the amplitude and phase computed from the tight-binding model to each of these Gaussian shaped orbitals. The momentum-space radiation pattern is obtained by Fourier transformation of this wave function. The state in Fig. S1(d), with a phase difference of π between neighboring plaquettes, corresponds to a Bloch state $|\psi(\pi/a)\rangle$, but truncated to only 4 unit cells.

Importantly the non-linear domains measured in our experiment indeed present a spatial pattern similar to the one calculated in Fig. S1(d). This pattern reflects the phase imposed by the drive at the edge of the BZ, resulting in low intensity on A sites inside the non-linear domains because of destructive interferences. A sites have significant intensity only at the edge of the domains or in regions where disorder overcomes interaction energy (like in Fig. 2(d) or Fig. 2(e) in the main text) and locally breaks the destructive interferences.

II. PARAMETERS FOR NUMERICAL SIMULATIONS

The discrete Gross-Pitaevskii equation introduced to model our experiments (Eq. (2) of the main text) is a set of $3N$ equations, that describe the time evolution of the polariton amplitude on each site. N is the number of unit cells in the lattice. The coupling terms $t_{n,m}$ between the different sites are linked to the coupling constant t and t' of the Lieb tight-binding Hamiltonian (Eq. (1) of the main text) as follows:

* valentin.goblot@c2n.upsaclay.fr

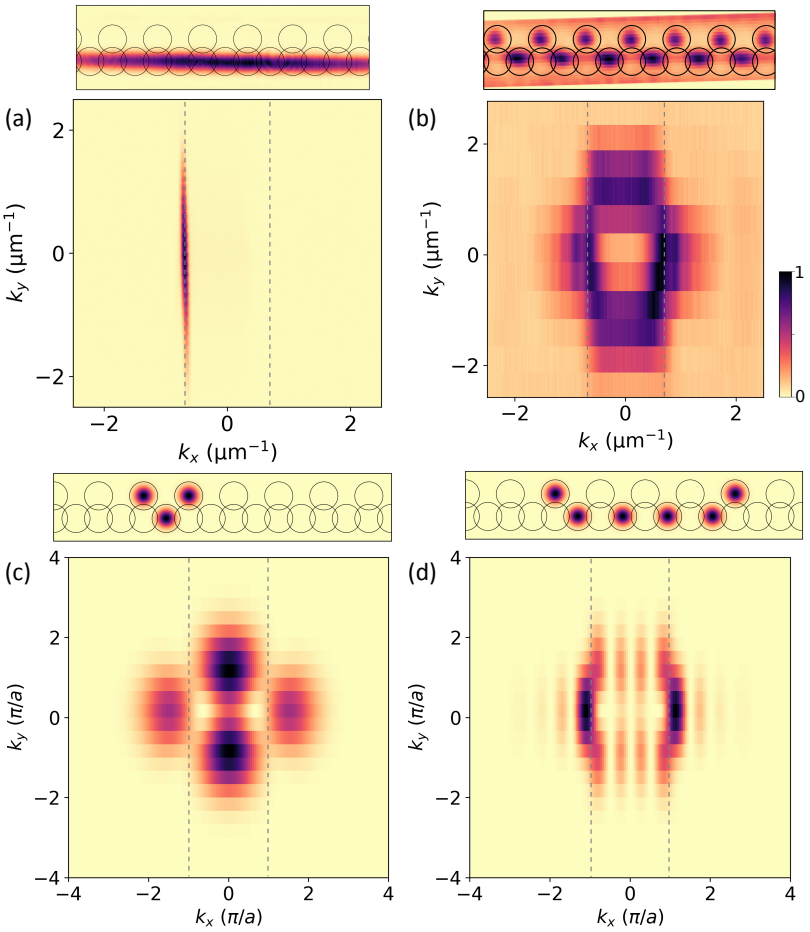

FIG. S1. (a) Real- (top) and momentum-space (bottom) images of the laser spot used for resonant excitation. (b) Measured real- and momentum-space photoluminescence at the flat band energy. (c,d) Calculated real- and momentum-space emission pattern of two examples of flat band eigenstates: (c) a single plaquette $|f_n\rangle$; and (d) a linear combination of four plaquettes with alternating sign on neighboring cells $\sum_{j=0}^{3}(-1)^j|f_{n+j}\rangle$. In all panels, dotted lines indicate the edges of the first Brillouin zone.

$$t_{nm} = \begin{cases} t & \text{if sites } n,m \text{ are neighboring } B \text{ and } C \text{ sites,} \\ t' & \text{if sites } n,m \text{ are neighboring } A \text{ and } B \text{ sites,} \\ 0 & \text{otherwise, i.e. if sites } n,m \text{ are not neighbors.} \end{cases} \quad (1)$$

The values of the parameters are deduced from the tight-binding fit to the measured polariton dispersion as shown in Fig. 1(c) of the main text. In the case of the flat band, we take $E_A = E_C = E_0$, $E_B = E_C - 10\gamma$ and $t = t' = 10\gamma$, with $\gamma = 30\mu$eV (and the energy offset $E_0 = 0$ for simplicity). For the dispersive band, we use $E_A = E_C + 6\gamma$, all other parameters being unchanged.

III. NUMERICAL SIMULATIONS: STEADY-STATE SPATIAL PROFILES

In this section we present the steady-state spatial intensity profiles calculated for the quasi-resonant injection of polaritons in the flat band, that correspond to the total intensity and domain size from Fig. 2(b,i) of the main text. The drive detuning is $\Delta = 3\gamma$ and the drive wave vector $k_p = \pi/a$. The calculated total intensity versus drive power F^2 from Fig. 2(b) of the main text is reproduced in Fig. S2(a). Fig. S2(b-d) shows the calculated spatial profile on pillars C for different values of F^2. In each case, a nonlinear domain delimited by a sharp drop in occupation at the edges is clearly identified. As F^2 is increased above the first abrupt intensity jump, each intensity jump corresponds to an increase of the domain size by exactly 1 unit cell (UC).

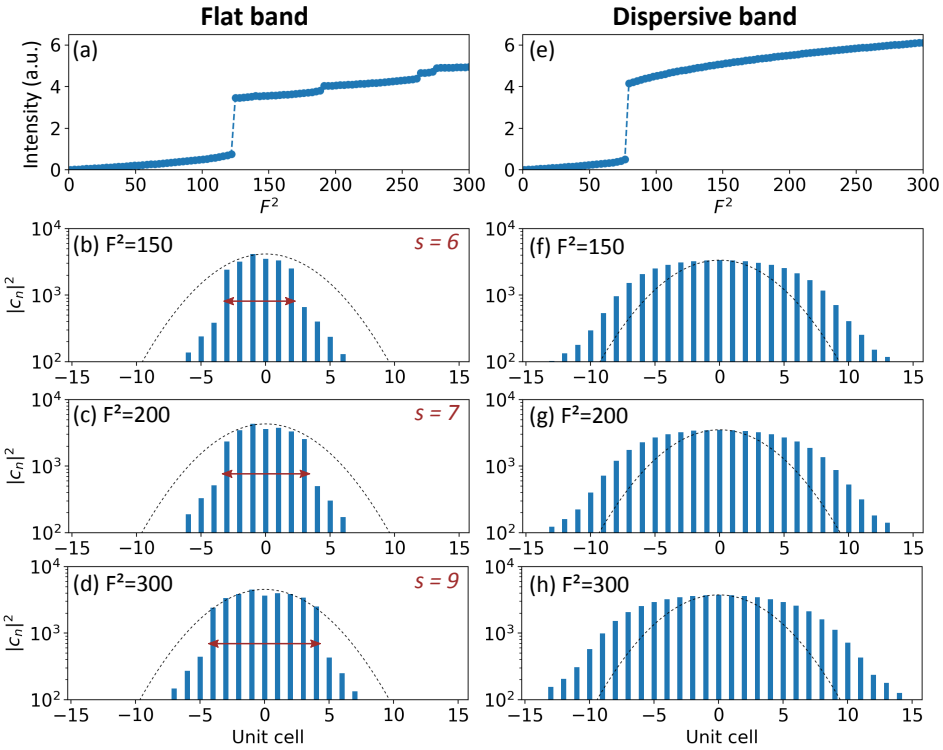

FIG. S2. **Comparison between the polariton non-linear dynamics in the flat and when driving the system within a dispersive band** : (a-d) calculation for the flat band with $E_A = 0$; (e-h) calculations for the dispersive band with $E_A = 6\gamma$; in both cases $\Delta = 3\gamma$. (a,e) Total intensity calculated as a function of F^2. (b-d, f-h) Steady-state occupation $|c_n|^2$ on sites C for various values of the drive intensities F^2. Dashed lines indicate the shape of the pumping spot. For panels (b-d), s is the domain size.

As a comparison, we repeat the numerical simulation with same excitation conditions ($\Delta = 3\gamma$, $k_p = \pi/a$), but with $E_A = 6\gamma$, such that the middle band is now dispersive and the drive frequency lies within the band. The results are presented in Fig. S2(e-h). As detailed in the main text, a single jump is observed in the calculated total intensity as the drive power F^2 is increased. Moreover, the spatial density profile in the nonlinear regime is smooth and does not evolve significantly as F^2 is increased.

IV. INFLUENCE OF DISORDER IN A FLAT BAND

As explained in the main text, we experimentally observe that the size of the nonlinear domain formed in the flat band can jump by several unit cells at a time when the pumping power is increased (see Fig. 2(h) of the main text, reproduced in Fig. S3(a)). This feature is not reproduced by the simulation (see Fig. 2(i) of the main text), where increases by one unit cell only are obtained (except for the first jump). In the following we show that disorder in the on-site energies can explain this discrepancy.

Disorder can strongly affect the physics of particles in a flat band, for example leading to the fragmentation of a bosonic condensate into plaquette-sized localized modes [1]. Indeed, since kinetic energy is zero in a flat band, any finite amount of disorder will break the flat band picture. In a dissipative context, disorder strength needs to be greater than the linewidth to significantly alter the physics. Experimentally, disorder mainly stems from small fluctuations in the pillar size and shape, caused by etching.

An estimate of the disorder strength can be extracted from resonant spectroscopy of the flat band eigenstates in the linear regime. Figure S3(b) shows the light intensity transmitted through A and C pillars when scanning the laser energy. When the laser is in resonance with an eigenstate, an intensity maximum is observed. The figure clearly indicates some spatial energy spreading of the eigenstates across the lattice. More precisely for this particular part of the chain, a redshift is observed to the left of UC 0, and to the right of UC 5. The maximal energy difference between the different states is around $80\,\mu$eV, comparable to the laser detuning $\Delta = 90\mu$eV used in Fig. S3(a) (and Fig. 2 of the main text). Thus in the experiments disorder strength is comparable to the interaction energy. Note that imaging

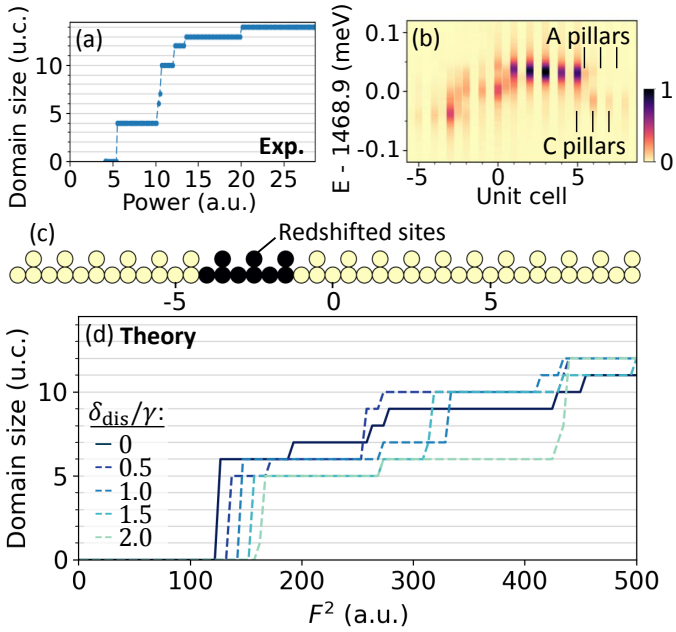

FIG. S3. **Influence of disorder on the nonlinear regime for the flat band.** (a) Measured size of the nonlinear domains as a function of excitation power (reproduced from Fig. 2(h) of the main text). (b) Measured intensity profile on pillars A, C as a function of resonant drive energy in the linear regime ($P = 10\mu$W). (d) Calculated size of the nonlinear domain for increasing excitation drive F^2, when including a redshift δ_{dis} on the sites indicated in black in (c). This redshift mimics the effect of local disorder in the chain.

of the eigenstates as done in Fig. S3(b) does not allow extracting precise on-site disorder on each individual pillar. Nevertheless, to get a flavor of the effect of disorder on the nonlinear domains, we introduce in our simulations a distribution of on-site energies which results in a distribution of eigenstates resembling the measured one. A redshift $\delta_{\rm dis}$ is introduced for the on-site energy of all sites on 2 UCs to the left of the excitation spot (see Fig. S3(c)). The corresponding simulation of the nonlinear domain size versus F^2 is shown in Fig. S3(d) for different disorder strengths. As in the experiment, we observe series of jumps of different amplitudes. For instance for $\delta_{\rm dis} = 0.5\gamma$, an abrupt jump from 6 to 9 UCs occurs at $F^2 \approx 250$. It corresponds to a progression of the domain edge through all redshifted sites at once. For stronger disorder amplitude, additional big jumps in the domain size are observed at higher excitation powers. The redshifted sites thus create a barrier for the domain edges, and modify the growth of the domains with power. In the experiment, the disorder landscape is certainly more complex but this simple simulation provides good understanding of the effect of disorder on the observed nonlinear dynamics. We have verified on several lattices realizing different disorder configurations that the nonlinear behavior reported here is qualitatively the same.

V. TRUNCATED BLOCH WAVES IN THE GAP ABOVE A DISPERSIVE BAND

We investigate with numerical simulations the behavior of a nonlinear fluid injected in the gap above a dispersive band. Figure S4(b-d) presents the steady-state profiles calculated in the nonlinear regime and without disorder, for $E_A = 6\gamma$ and different values of the drive energy detuning with respect to the bottom of the middle band: $\Delta = 4$, 5 and 7γ. Note that for $E_A = 6\gamma$, the width of the middle band is $\sim 4.6\gamma$, so that when $\Delta > 4.6\gamma$ the drive lies within the gap. For $\Delta = 4\gamma$, i.e. for a drive below the band edge, the propagation outside the spot is visible as a spatial exponential decay of the intensity. The propagation length L characteristic of the spatial decay is given by $L = v_g/\gamma$, with $v_g = \hbar^{-1}(\partial E/\partial k)$ the group velocity at energy Δ. Increasing the drive energy to $\Delta = 5\gamma$, a sharp spatial decrease in the intensity is now observed at UC ± 11. For $\Delta = 7\gamma$, further into the gap, the domain edge is even sharper. In this excitation configuration, since the drive injects polaritons within the gap, there is no single-particle state at this energy. As a result, the interaction energy provided by the drive cannot be converted into kinetic energy: propagation of particles out of the excitation region is prevented. This localization mechanism arising from the interplay between interactions and the existence of an energy gap is precisely the one at play in the formation of gap solitons, and in particular of Truncated Bloch Waves, as originally discussed in Refs. [2–4].

Thus when the dispersive band is excited within the gap at high energy, Truncated Bloch waves are excited in a

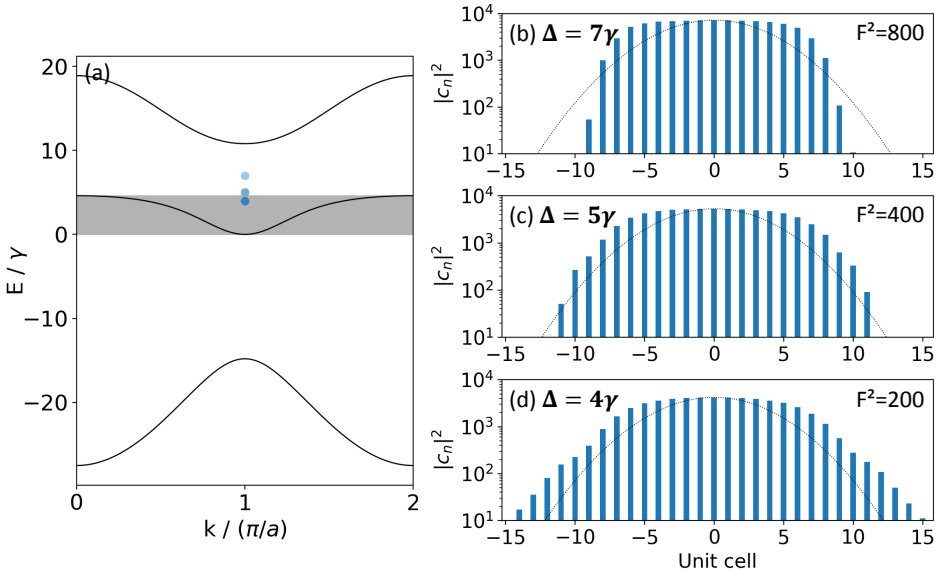

FIG. S4. (a) Band structure calculated by diagonalization of the tight-binding Lieb Hamiltonian for $E_A = 6\gamma$, $E_B = -10\gamma$ and $E_C = 0$. The shaded gray region indicates the total spectral width of the middle band. Blue dots indicate the drive energy and wave vector used in panels (b-d). (b-d) Steady-state occupation $|c_n|^2$ on sites C calculated for different values of Δ, in the nonlinear regime (for a value of F^2 indicated in each panel).

similar way as for the flat band. The energy injected in the system is larger than the maximum kinetic energy the system can accommodate so that non linear domains with sharp edges are formed. In the flat band, since kinetic energy is strictly zero, this regime is achieved as soon as the driving energy overcomes the other energy scales of the system, namely the spectral linewidth and disorder.

VI. MULTISTABILITY OF THE NONLINEAR DOMAINS

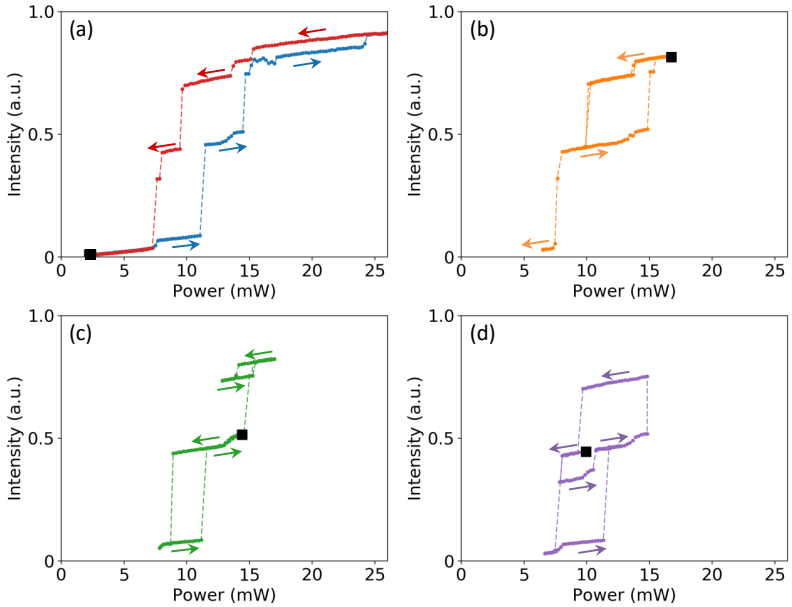

FIG. S5. (a-d) Total emission intensity measured under resonant excitation of the flat band for different the power scans. In each panel, the starting excitation condition is denoted by a black square and arrows indicate the scan direction.

In Fig. S5 we present several experimental power scans obtained with excitation parameters similar as those used in Fig. 2 of the main text ($\Delta = 90$ μeV and $k_p = \pi/a$). For each of these power scans, the starting condition is denoted by a black square. Fig. 3(a) of the main text reproduces all these measurements on top of each other.

VII. INFLUENCE OF DISORDER WITHIN A DISPERSIVE BAND

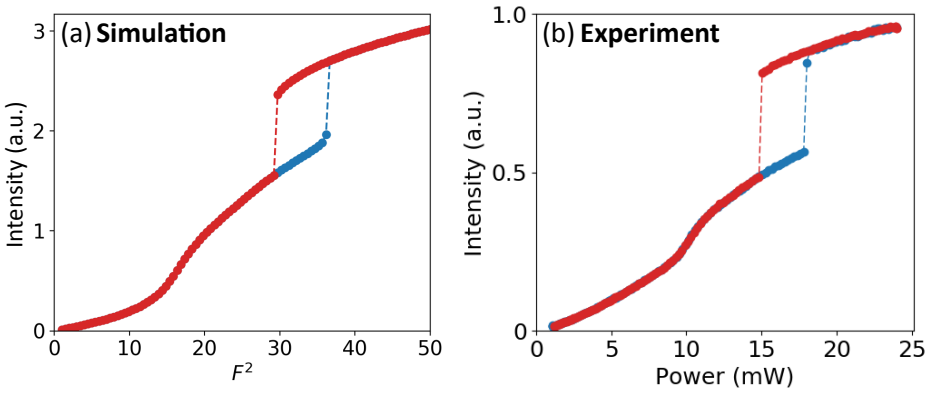

FIG. S6. **Influence of disorder on the nonlinear regime for the dispersive band.** (a) Calculated total intensity in the lattice versus F^2, for an increasing (blue) and decreasing (red) drive intensity. The redshift amplitude is $\delta_{\rm dis} = 2\,\gamma$ on the same sites as for the flat band, and the drive detuning $\Delta = 1.5\gamma$. (b) Total emission intensity measured in the dispersive band as a function of excitation power (reproduced from Fig. 4(a) from the main text).

Disorder also has an influence on the nonlinear regime in the dispersive band. This is due to the fact that the disorder amplitude in the experiment, on the order of 80 μeV, is comparable to the interaction and kinetic energy of the fluid with our choice of laser detuning $\Delta = 60$ μeV. In Fig. S6, we present the results of a numerical simulation taking into account disorder in the dispersive band: we introduce a redshift $\delta_{\rm dis} = 2\gamma$ on the same sites as in Fig. S3(c), $\Delta = 1.5\gamma$ and $E_A = 6\gamma$. The total population versus F^2 in the up and down scans are in excellent agreement with the experimental results from Fig. 4(a) of the main text, reproduced in Fig. S6(b). Indeed, the presence of disorder explains the first nonlinear increase in the total intensity before the abrupt jump (only one jump was observed in disorder free simulations, see Fig. 4(b) of the main text).

[1] F. Baboux, L. Ge, T. Jacqmin, M. Biondi, E. Galopin, A. Lemaître, L. Le Gratiet, I. Sagnes, S. Schmidt, H. E. Türeci, A. Amo, and J. Bloch, Phys. Rev. Lett. **116**, 066402 (2016).
[2] T. J. Alexander, E. A. Ostrovskaya, and Y. S. Kivshar, Phys. Rev. Lett. **96**, 040401 (2006).
[3] T. Alexander and Y. Kivshar, Applied Physics B **82**, 203 (2006).
[4] J. Wang, J. Yang, T. J. Alexander, and Y. S. Kivshar, Phys. Rev. A **79**, 043610 (2009).